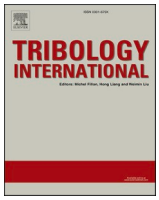
Tribology International 227 (2027) 112870



Contents lists available at ScienceDirect

Tribology International

journal homepage: www.elsevier.com/locate/triboint



Full length article

Pre-graphitized interface enables macroscopic superlubricity of Si-DLC:H coating

Yupeng Zhang [a,1], Silong Zhang [a,1], Yanjin Li [a], Rende Chen [a,*], Gang Wen [c], Ming Qin [c], Peng Guo [a], Dae-Eun Kim [d], Hao Li [a], Aiying Wang [a,b,**]

[a] State Key Laboratory of Advanced Marine Materials, Zhejiang Key Laboratory of Extreme-environmental Material Surfaces and Interfaces, Ningbo Institute of Materials Technology and Engineering, Chinese Academy of Sciences, Ningbo, Zhejiang, 315201, China
[b] Center of Materials Science and Optoelectronics Engineering, University of Chinese Academy of Sciences, Beijing, 100049, China
[c] Guangdong Meizhi Compressor Co., Ltd., Foshan, Guangdong, 528000, China
[d] Department of Mechanical Engineering, Yonsei University, Seoul, 03722, Republic of Korea

ARTICLE INFO

Keywords:
DLC
Tribology
Superlubricity
Graphitization
Friction interface

ABSTRACT

Although superlubricity in silicon-doped hydrogenated diamond-like carbon coatings can enhance mechanical energy efficiency, but it is heavily dependent on special conditions, high contact loads and inert atmospheres. In this work, we proposed a strategy that combines pre-graphitization with tailored counterpart material to construct a weak chemically bonded interface for superlubricity. The fabricated Si-DLC:H coating exhibits high adhesion and mechanical properties (H=17.5 GPa, E = 130 GPa), enabling stable superlubricity (COF=0.009 ± 0.5‰) under N_2. Friction-induced graphitization occurs concurrently with the formation of powdery wear debris, SiO_x nanoparticles dispersed in a sp^2-rich loose layer on the wear track. This debris forms a distinctive friction interface characterized by weak chemical bonding and low shear strength, ultimately leads to superlubricity. Supported by RMD simulations, this study provides a comprehensive understanding of the dynamic evolution of friction interface. It breaks through the conventional graphitization mechanism, and clarifies the macroscopic superlubricity mechanism from the perspective of weak chemical bond breaking and graphitization.

1. Introduction

As the global industrial system accelerated transition toward a green and low-carbon future, improving the energy efficiency and reliability of mechanical systems has become key to conserving energy and reducing emissions. Friction and wear in critical components, such as air conditioning compressors and bearings, lead to significant energy waste and equipment failure [1,2]. Superlubricity technology, defined as a sliding states that the friction between two contact surfaces approaches zero, characterized by a coefficient of friction (COF) lower than 0.01 in the engineering field [3,4], which is a revolutionary solution to break through the performance limits of traditional lubrication technology, extending service life and lowering energy consumption of mechanical.

Diamond-like carbon (DLC) coatings consist of an amorphous network of covalently bonded carbon atoms with mixed sp^3 (diamond-like) and sp^2 (graphite-like) hybridization [5,6]. This unique structure confers high hardness, excellent wear resistance and low COF to DLC coatings [7]. Recent studies have demonstrated that hydrogenated DLC coatings can achieve macroscopic superlubricity in dry inert atmospheres [8,9]. DLC:H coatings are not intrinsically superlubricious, however, they may exhibit superlubricity behavior in certain cases, which is primarily explained by the graphitization-transfer film mechanism. Under high shear stress, friction induces the transformation of a disordered sp^3-C network into an ordered, layered sp^2-C nanocluster structure. Simultaneously, a transfer film forms on the counterpart, creating a weakly interacting interface that leads to superlubricity [10–12].

Nevertheless, attaining macroscopic superlubricity of DLC:H

* Corresponding author.
** Corresponding author at: State Key Laboratory of Advanced Marine Materials, Zhejiang Key Laboratory of Extreme-environmental Material Surfaces and Interfaces, Ningbo Institute of Materials Technology and Engineering, Chinese Academy of Sciences, Ningbo, Zhejiang 315201, China.
E-mail addresses: chenrd@nimte.ac.cn (R. Chen), aywang@nimte.ac.cn (A. Wang).
[1] These authors contributed equally to this work

https://doi.org/10.1016/j.triboint.2026.112870
Received 22 May 2026; Received in revised form 3 October 2026; Accepted 18 October 2026
Available online 19 October 2026
0301-679X/© 2026 Elsevier Ltd. All rights are reserved, including those for text and data mining, AI training, and similar technologies.

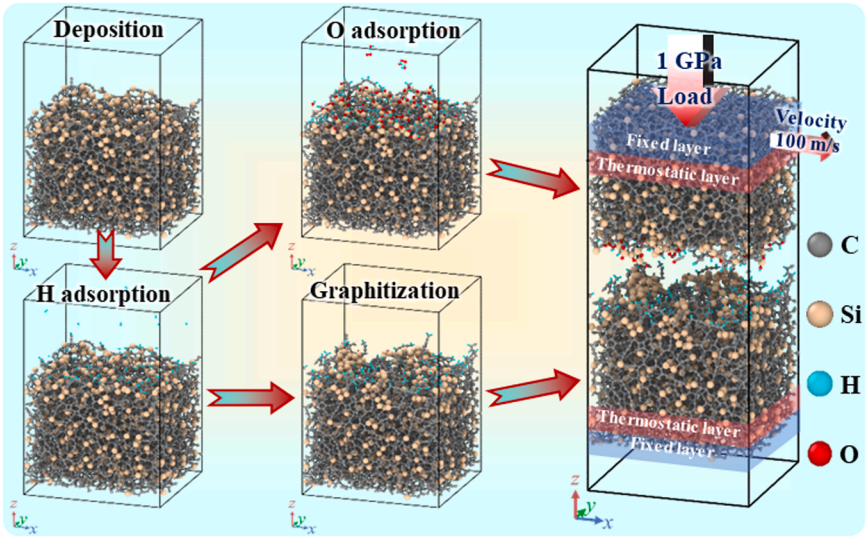


Fig. 1. Schematic diagram of friction model construction process.

coatings remains a well-recognized challenge. Moreover, owing to the instability of graphitization that dependence on high Hertz contact stress, and the expulsion of transfer film, DLC:H coatings falling long-term engineering requirements. Additionally, these coatings often suffer from high residual stress and poor film-substrate adhesion. Excessive contact pressure leads to over-graphitization and thinning of the transfer film, promoting crack initiation and spallation [13–15], while insufficient contact pressure fails to induce graphitization. Consequently, establishing a superlubricious interfacial structure or low interface shear strength is difficult, resulting in a high COF.

For addressing these challenges, Chen et al. modulated plasma energy to alter the sp^2 cluster structure in DLC:H coatings and identified high Hertz contact stress as the factor triggering the conversion of sp^3-C to sp^2-C transfer film, this enabled macroscopic superlubricity in N_2 environment [5,13,16]. Wang et al. prepared Si-DLC:H coatings to *reduce internal stress and enhance film-substrate adhesion,* the Si reacts with moisture that promotes the formation of curved graphene-like structures and achieve superlubricity [17–19]. *The adopted Si also facilitates the transformation of sp^3-C to sp^2-C, effectively diminishing atomic-scale interactions at friction interface that more prone to shear*[20,21]. Li et al. demonstrated that in situ graphitization of coating increases the *highly* ordered *sp^2-C* and reduces surface dangling bonds, while the interfacial bonding state shifts from covalent to weak molecular interactions, enhancing repulsive forces and enabling superlubricity [22]. Ji et al. discovered that low interfacial activity of counterpart facilitates the generation of onion-like carbon nanoparticles at the friction interface, shielding dangling bond interactions and achieve superlubricity [9, 23]. *Nevertheless, the precise structure responsible for superlubricity remains unclear, and correlating the evolution of bonding states with macroscopic* superlubricity *is challenging.*

This study employs high-power pulsed magnetron sputtering (HiPIMS)-assisted ion beam technology to fabricate Si-DLC:H coatings with high strength and toughness. A pre-graphitization strategy is applied to increase the sp^2-C content of coating. During friction, the formation of a low-shear-strength friction interface contributes to the realization of superlubricity. Notably, achieving superlubricity of the Si-DLC:H coating in an engineering evaluation is of great interest in this study. Reactive molecular dynamics simulation is utilized to reveal the dynamic evolution of the friction interface from an atomic structure perspectiv. In particular, this work integrates weak chemical bonding theory with the graphitization mechanism to refine the existing superlubricity framework and elucidate the underlying tribology mechanism of Si-DLC:H coatings.

2. Experimental and computational details

2.1. Preparation of coatings

The ion beam-assisted HiPIMS technology was utilized to fabricate Si-DLC:H coatings. Prior to deposition, the 316 stainless steel substrate (Ra=0.3 μm) and Si (111) wafers underwent ultrasonic cleaning in acetone and ethanol solutions for 20 min. After drying, samples were mounted onto the holder and loaded into the deposition chamber. The chamber was evacuated to 5×10^{-5} Pa, subsequently, samples were subjected to Ar^+ ion etching for 30 min at a negative bias voltage of −200 V to remove surface impurities. Subsequently, an Cr/AlCrSiCN transition layer was deposited by HiPIMS technique using an Cr and AlCrSi targets with a duty cycle of 2%. The Cr layer was deposited 5 min under the bias voltage of −200 V and Ar flow rate of 90 sccm. The AlCrSiCN layer was deposited 20 min under the bias voltage of −100 V, Ar flow rate of 90 sccm, N_2 flow rate gradually decrease from 30 sccm to 0, C_2H_2 flow rate gradually increase from 0 to 30 sccm. Following this, the HiPIMS power was switched off while the ion beam source was activated with a bias voltage of −100 V. CH_4 gas was introduced at a flow rate of 27 sccm, along with tetramethylsilane ($C_4H_{12}Si$) gas at 9 sccm, for 300 min to fabricate a Si-DLC:H coating. After deposition, the samples were annealed at 300 °C for 30 min under vacuum (5×10^{-5} Pa) in a Rapid Annealing Furnace, with a heating rate of 30 °C/min, and then cooled naturally to room temperature (the heating and cooling curves shown in Fig. S1).

2.2. Tribology test

The tribological behaviors of coatings were evaluated using a ball on disk tribometer (Anton Paar, Switzerland). Prior to testing, the instrument was calibrated to ensure experimental precision and accuracy. A GCr15 ball with a radius of 6 mm, coated with DLC or DLC:H-SiO coatings respectively, served as the counterpart to investigate the influence on the tribological performance of coating. The test conditions were set as follows: rotational speed of 0.4 m/s, radius of 5 mm, frequency of 50 Hz, load of 2 N (average Hertz contract pressure is about 0.53 GPa) [13], and the total cycles are 82000. The testing chamber was enclosed and purged with dry N_2, relative humidity was reduced below 5%, after which the tribological testing was started.

The depth and width of the wear tracks were measured using a surface profilometer, and all coatings were measured at least 5 times. The wear rate (W_R) was subsequently calculated using formula (1):

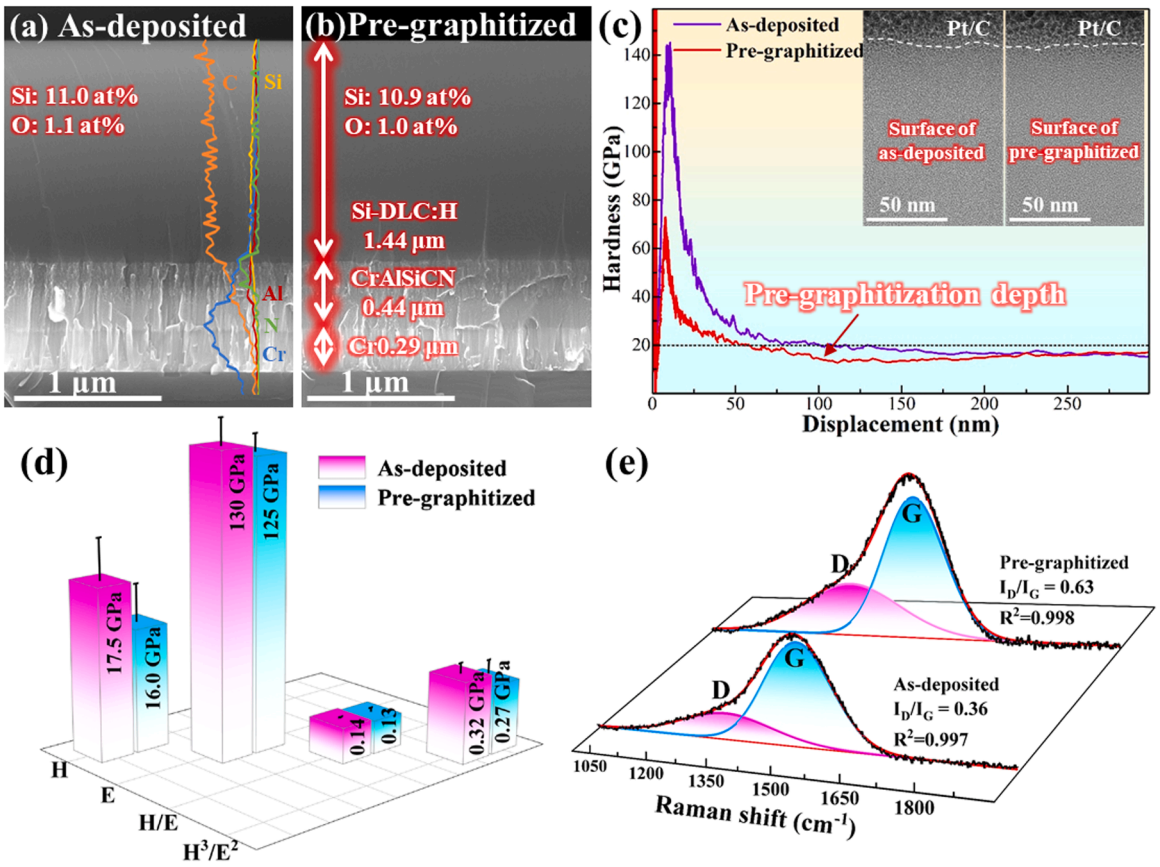


Fig. 2. Cross-sectional morphology of as-deposited (a) and pre-graphitized (b) Si-DLC:H coating, displacement-hardness curves (c), mechanical properties (d), Raman peaks (e).

$$W_R = V/(F_n \times S) \quad (1)$$

Where V is the wear volume (mm^3), Fn is the normal load (N), and S is the sliding distance (m). To minimize experimental error, a minimum of five replicate measurements were performed for each sample, and the average wear rate was reported.

2.3. Reactive molecular dynamics simulation

The Large-scale Atomic/Molecular Massively Parallel Simulator (LAMMPS) was employed to carry out reactive molecular dynamics (RMD) simulations [24,25]. The RMD method was utilized to construct the atomic models of DLC:H-SiO counterpart, as-deposited and annealed Si-DLC:H coating. Detailed information about the simulation models is provided in Fig. S2–3. The Fig. 1 shows the schematic diagram of friction interface model of as-deposited and pre-graphitized Si-DLC:H with DLC:H-SiO counterpart, with a size of 46.37 × 42.83 × 120.00 $Å^3$. In this model, the outermost atomic layer (5 Å thickness) were held rigid, while the bottom and top layers with (10 Å thickness) are maintained at a constant at 300 K, all remaining atoms were unconstrained [26]. Our team [27,28] and other studies [29,30] have confirmed that the application pressure of 1 GPa to the top rigid layer over 50 ps was suitable for investigating friction behavior at the atomic scale [31]. Due to the short time scale of MD simulations, a long sliding distance is required to achieve effective structural sampling, a constant velocity of 100 m/s was applied along the x-direction, enabling the system to slide under a fixed pressure [32,33]. A fixed pressure is exerted on the top rigid layer to maintain continuous sliding for 1250 ps, ensuring the system reaches a steady friction state. During the friction process, periodic boundary conditions were applied along the x- and y-directions, and the molecular dynamics time step is set to 0.25 fs. Atomic interactions within the system are described using the Reactive Force Field [34], which incorporates the concept of bond order to account for instantaneous atomic interactions. This approach allows for covalent bond formation and dissociation, and chemical reactions in complex carbon-based systems, with accuracy comparable to quantum calculations.

2.4. Characterization methods and instruments

The morphology of cross-sectional, surface and wear track were characterized by the thermal field scanning electron microscopy (SEM, Verios G4), the composition was analyzed using the accompanying energy dispersive spectrometer (EDS). The confocal microraman spectrometer (Raman, Renishaw inVia Reflex), with the excitation wavelength of the laser being 532 nm, was used to analyze the chemical composition and structure. The evolution in the bonding state structure of coatings before and after friction tests were investigated using X-ray photoelectron spectroscopy (XPS). Samples for TEM were prepared by focused ion beam scanning electron microscopy (FIB, Auriga). The microstructure of coating was characterized by transmission electron microscopy (TEM, Talos F200x). The mechanical properties of the coating were tested by nano-indentation tester (MTS NANO G200). The surface profiler (KLA-Tencor Alpha-Step IQ) was used to measure the depth and width of the wear track and calculate wear rate.

3. Results and discussion

3.1. Morphology and mechanical properties

The cross-sectional morphology shown in Fig. 2a-b primarily consists of an Si-DLC:H top layer with a thickness of 1.44 μm, the line scanning shows a gradient transition layer of Cr/CrAlSiCN with a thickness of

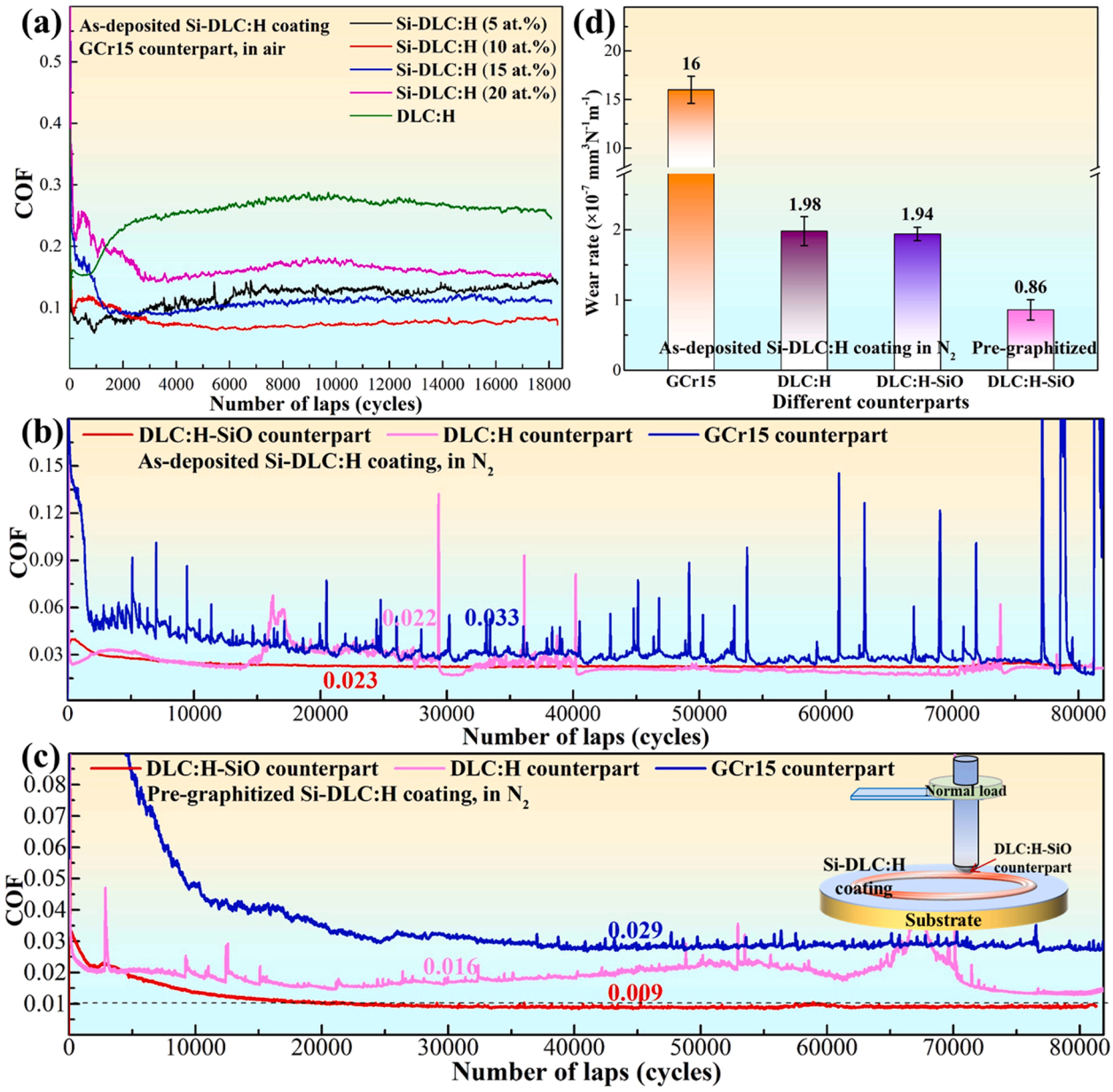


Fig. 3. COF of as-deposited Si-DLC:H coatings in air (a), with different counterparts in N_2 (b), COF of pre-graphitized coatings with different counterparts in N_2 (c), and wear rates (d).

0.73 μm to enhance the adhesion strength between film and substrate. The as-deposited Si-DLC:H functional layer (Si-11.0 at%) exhibits a similar dense internal structure to pre-graphitized coating, and tightly bonded to the columnar crystal transition layer. This structure alleviates mismatch and hardness gradients at the interface between the coating and the substrate, thereby enhancing adhesion. After pre-graphitization, the content of C on the coating surface increases, while the Si and O contents decrease slightly. The scratch test in Fig. S4 shows that no significant spallation is observed even at the end of scratch track, and the Lc3 value exceeding 60 N demonstrates strong adhesion.

Fig. 2c shows that the initial hardness (H) of the pre-graphitized coating is lower than that of the as-deposited coating. As the indentation depth increases, the hardness decrease and eventually tending to be similar, this suggests that the graphitization depth is around ~100 nm. The inserted TEM micrograph shows only minor differences in structural features. Fig. 2d shows the H of as-deposited coating is 17.5 GPa and the elastic modulus (E) is 130 GPa. Influenced by the graphitization of the surface nanolayer, the H and E of pre-graphitized coating show a slightly decrease, 16.0 GPa and 125 GPa, respectively. The H/E and H^3/E^2 are positively correlated with fracture resistance and plastic deformation resistance, respectively. Higher values indicate enhanced mechanical properties, greater capacity to withstand stress and strain, reduced crack initiation and improved wear resistance [35,36]. The H/E and H^3/E^2 values of as-deposited coating are 0.14 and 0.32 GPa, slightly higher than that pre-graphitized coating, indicating good mechanical properties and wear resistance.

The carbon bonding states of both Si-DLC:H coatings were characterized by Raman spectroscopy, as shown in Fig. 2e. In each spectrum, the deconvolutions were performed by the Gauss method with Savitzky-Golay smoothing. The G peak around 1540 cm^{-1} is attributed to the stretching vibrations of sp^2-C atom pairs (C-C, C=C) and π-electrons in carbon aromatic rings or chains. The D peak at 1348 cm^{-1} is assigned to the breathing vibration mode of sp^2-C atoms in disordered hexagonal brillouin zones [18]. Its intensity reflects the proportion of defects, structural distortions, and amorphous regions in the coating. The higher intensity of G peak compared to D peak indicates fewer defects and

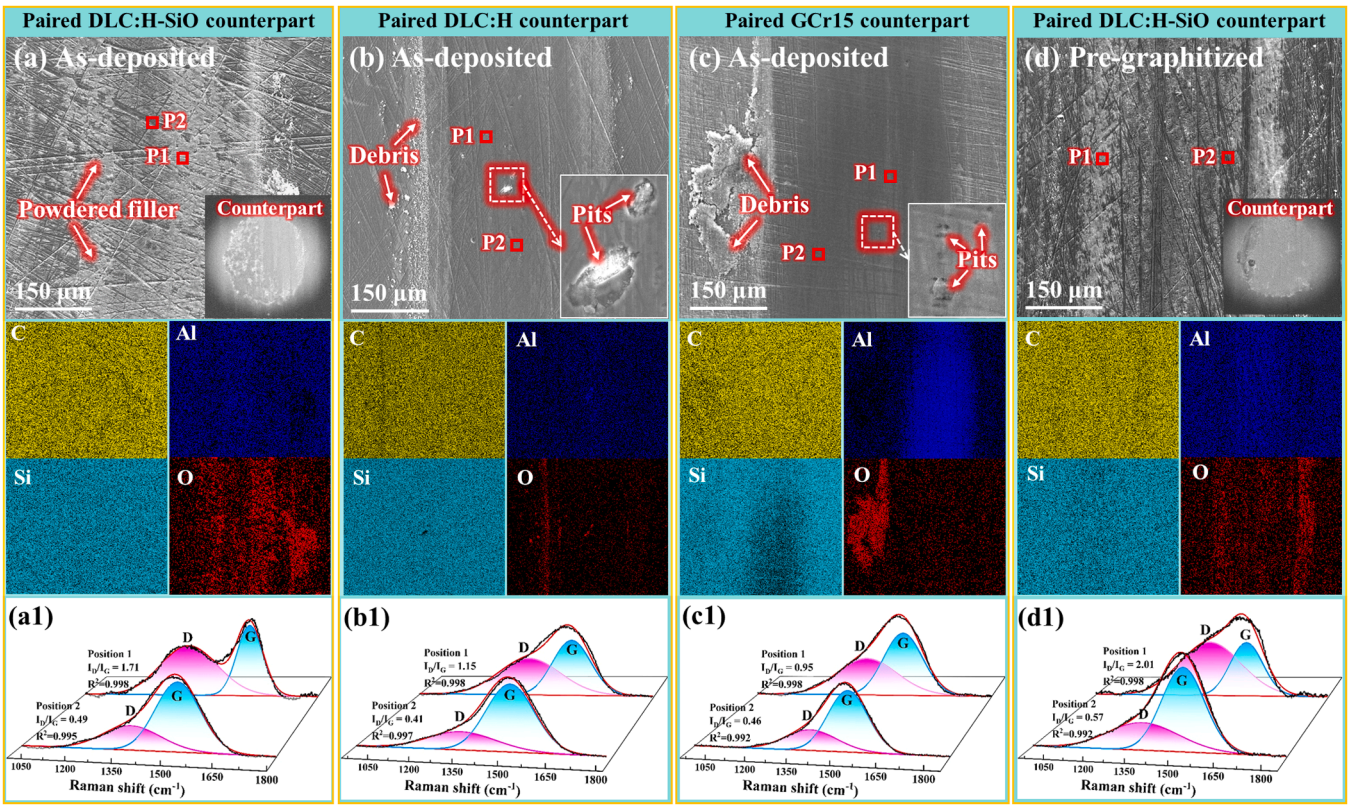


Fig. 4. The morphology of wear track, EDS and Raman peaks of the as-deposited and pre-graphitized Si-DLC:H coating corresponding to DLC:H-SiO (a, a1), DLC (b, b1), GCr15 (c, c1) and DLC:H-SiO counterparts (d, d1).

better coating quality in Si-DLC:H coating. The area ratio of the D and G peaks (I_D/I_G) shows a linear relationship with the sp^2/sp^3 ratio and the degree of graphitization [5,37]. The full-width half maximum (FWHM) reflect the sp^2 nanoclusters size or in-plane correlation length (La) of the amorphous carbon film according to the formula (2) [38]:

$$I_D/I_G = C(\lambda)/La \quad (2)$$

Where C is a constant of 0.0055, La is the sp^2-C nanocluster size. A comparison reveals that the pre-graphitization process leads to an increase in the I_D/I_G area ratio to 0.63, with an adjusted R^2 of 0.994, indicating the growth of sp^2-C nanoclusters and reorganization of the carbon network due to hydrogen loss.

3.2. Tribological properties

Fig. 3a shows the highest COF of pure DLC:H coating is 0.275 in atmospheric environment. In contrast, the coating with 10 at% Si exhibited the lowest COF of 0.07 along with a stable curve that was selected for further investigation. Fig. 3b reveals significant differences in the stability of friction curves against various counterparts in N_2 environment. The coating against GCr15 counterpart exhibits the highest and considerable fluctuations COF, the initial COF is 0.142 and drops rapidly to 0.058 after the run-in period and eventually stabilizes around 0.038. When sliding against the DLC:H counterpart, the COF of the coating remains low during the run-in period, then rises sharply and stays high until a stable stage is reached, with a final average COF of ~0.022. By contrast, the friction curve against the DLC:H-SiO counterpart stabilizes rapidly, with the COF dropping from 0.04 to 0.023, indicating superior friction performance. For the pre-graphitized Si-DLC:H coating (Fig. 3c), the initial COF against DLC:H-SiO is 0.032, which decreases during the run-in period to 0.009 ± 0.5‰ at 18,000 laps. The friction curve remains exceptionally smooth and stable, and the test endures over 82,000 laps without failure, achieving long-term superlubricity in N_2.

In comparison, when sliding against GCr15 counterpart, the COF gradually decreased from 0.28 and eventually stabilized at an average of ~0.029, showing little fluctuation. In contrast, against DLC:H, the COF initially decreases and then increased gradually, eventually reaching a minimum of 0.013, with a mean COF of 0.016. These COF values are notably lower than those of the as-deposited coatings, and the corresponding friction curves are also more stable, indicating that the pre-graphitized coating exhibits superior friction-reduction performance.

Fig. 3d presents the W_R of coatings against different counterparts. The severe wear of coating is against GCr15 counterpart that the W_R reached 16×10^{-7} mm^3/N·m. However, after depositing DLC:H and DLC:H-SiO coatings on the GCr15 ball, the W_R of Si-DLC:H coatings decreased significantly by an order of magnitude in atmospheric environment. Comparatively, the pre-graphitized coating exhibited the lowest W_R of 8.6×10^{-8} mm^3/N·m after friction in N_2 environment, demonstrating that DLC-based counterpart materials contribute to achieving superlubrication and low W_R of coatings.

3.3. Friction behavior of coatings

To elucidate the tribological behavior of Si-DLC:H coating, the wear tracks were characterized similar widths but distinct morphologies. Fig. 4a displays the wear track filled with powdery debris pairing with a DLC:H-SiO counterpart, indicating slight wear that consist of diverse position1 and position2 areas. The corresponding EDS reveals a uniform distribution of C and Si elements on the surface, oxygen is primarily concentrated in the central powdery fillers debris, suggesting the adhesive wear mechanism. Although the frictional heat generated during friction process, but the N_2 environment prevent oxidation from atmospheric, hence, it is inferred that the O elements originate from the DLC:H-SiO counterpart as shown in the insert of Fig. 4a. The Raman spectral

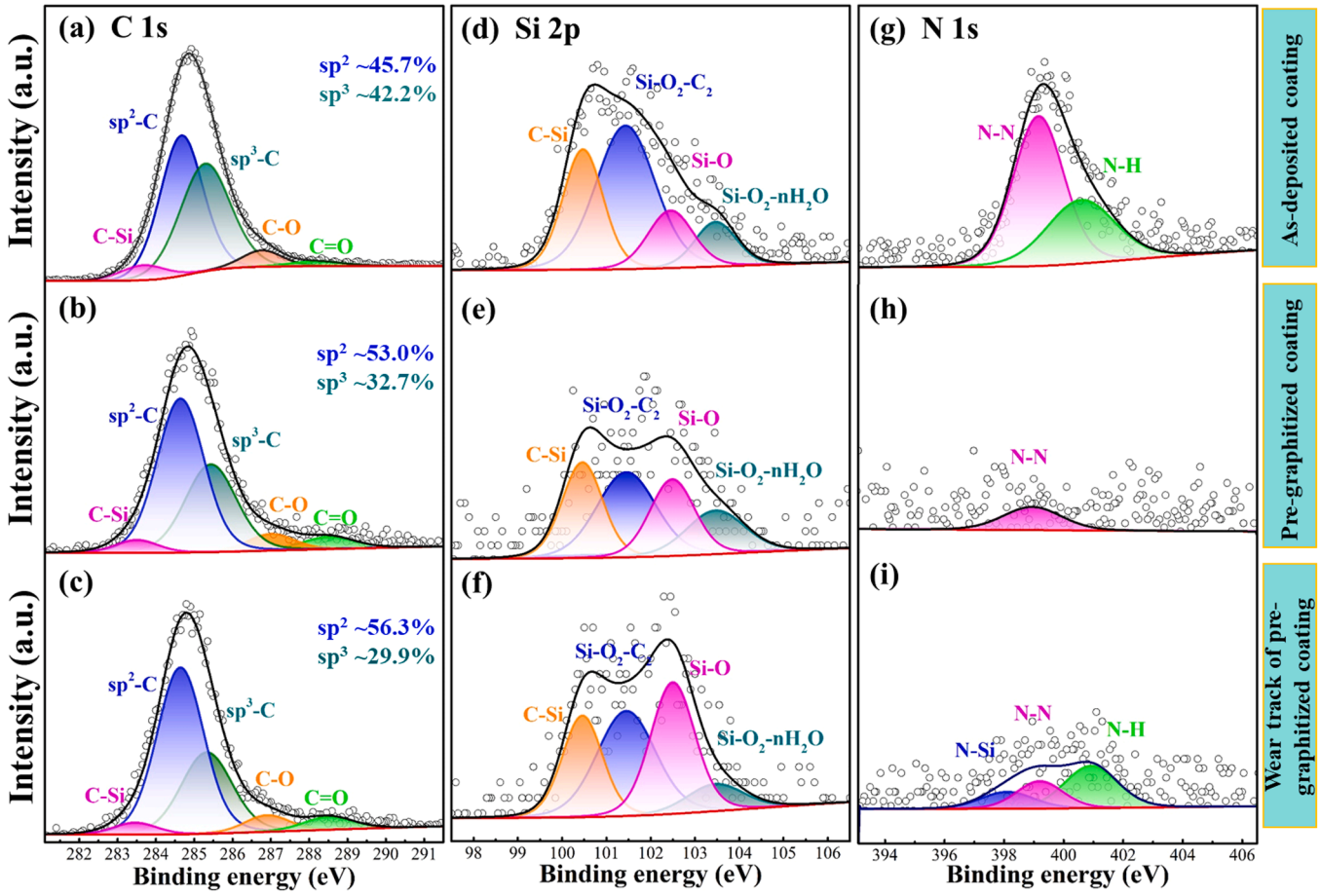


Fig. 5. Fine spectra of C1s, Si2p and N1s in deposited Si-DLC:H coatings (a, d, g), pre-graphitized coatings (b, e, h), and wear track (c, f, i).

shown that the I_D/I_G values of P1 area are higher than P2 area of all coatings, which means P1 area is primarily load-bearing and play a more crucial role in providing lubrication than P2 area. Fig. 4a1 shows the Raman peaks at P1 area that split D and G peaks, the increased I_D/I_G value to 1.71 indicates a rise in both sp^2-C content and nanocluster size within the wear track, which exhibits low bonding strength and is readily sheared under hertz contact stress, thereby acting as a sustained lubricating phase in contributing to a low and prolonged stable COF [39].

It is observed from Fig. 4b that scratches and protrusions were worn flat within the track pairing with DLC:H counterpart, while coating material was sheared off and delaminated in multiple areas, forming varying sizes pits. Wear debris accumulated on both sides, indicating that adhesive wear and abrasive wear is the dominant mechanism. The almost no O element detected by EDS can be attributed to the absence of oxygen in DLC:H counterpart. Fig. 4c shows significant depression and smooth in the central wear track against GCr15 counterpart, accompanied by numerous ploughing grooves and minor pores at localized regions. EDS showed a pronounced Al element from interlayer, while Si content decreased indicating severe wear of coating. Additionally, iron oxide-dominated debris accumulated, suggesting that oxide layers from GCr15 counterpart were worn off and adhered to the track, the wear mechanisms were primarily adhesive and mechanical wear. Fig. 4b1-c1 shows lower I_D/I_G values at both areas after friction, implying low-graphitization and insufficient lubricating phases, thereby resulted in substantial fluctuations and high COF.

The Fig. 4d shown the powdery debris formed in the pre-graphitized coating paired with DLC:H-SiO counterpart that providing stable and effective lubrication. Corresponding EDS indicates that oxygen is distributed within the debris region, co-localized with C and Si. This suggests that debris originates primarily from the counterpart, as illustrated in the insert of Fig. 4d. The Fig.4d1 reveals the highest I_D/I_G value of 2.01 at P1 area, with an adjusted R^2 of 0.999. The reduction in the FWHM of G peak indicates that, building upon the existed graphitic structure, friction further induces the formation of additional layered graphite-like carbon [11]. This process reduces the disorder of hybrid carbon, facilitating the establishment of a weakly chemically bonded friction interface between graphitized surface and counterpart, which is a key factor enabling the coating to achieve superlubricity. Furthermore, based on the wear track morphology and the I_D/I_G values at different regions, the sp^2-C generated primarily in the severely worn region during friction, serving as the main lubrication zone.

3.4. *The evolution of bond structure*

To elucidate the influence of chemical bonding evolution on superlubricity, XPS was employed to characterize the as-deposited, pre-graphitized Si-DLC:H coatings and wear track surface. All the characteristic peaks were calibrated with standard peak (284.8 eV), followed by background subtraction and Voigt function fitting under the similar FWHM and positions. Fig. 5a shows the C 1 s spectrum of as-deposited coating, which was divided into five peaks corresponding to C-Si, sp^2-C, sp^3-C, and C-O and C═O species [40,41]. The respective contents of sp^2-C, sp^3-C and C-Si were 45.7%, 42.2% and 4.4%. For the pre-graphitized coating in Fig. 5b, the sp^2-C content increased to 53.0%, while sp^3-C content decreased to 32.7%, resulting in raised sp^2-C/sp^3-C ratio that indicating an enhanced surface graphitization. Due to high-vacuum annealing, partial C-Si bonds broken, resulting in a reduced content of 3.98%. The content of C-O and C═O bonds of the pre-graphitized coating increased, and this is attributed to the

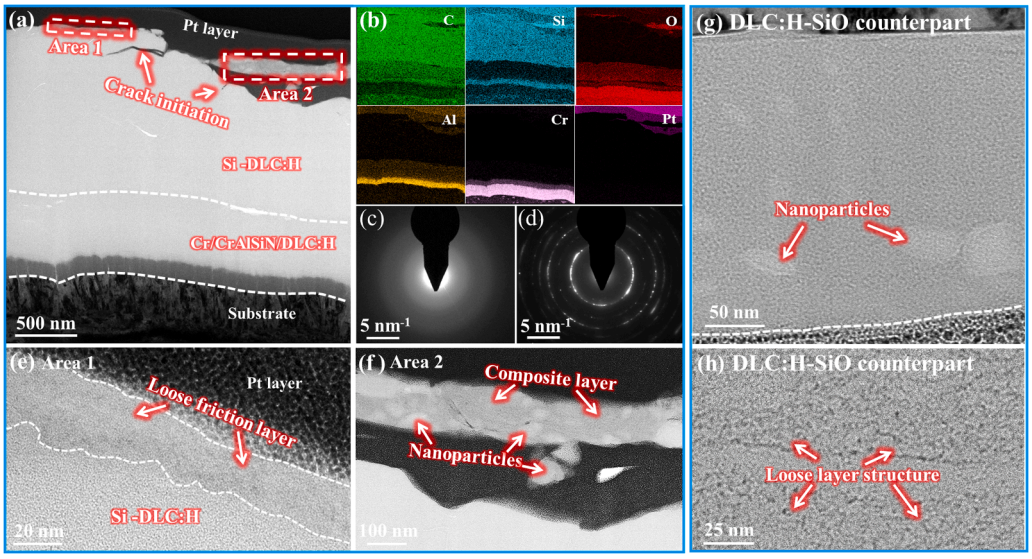


Fig. 6. Microstructure within wear track of pre-graphitized Si-DLC:H coating (a), mapping (b), diffraction patterns of upper layer and transition layer (c-d), local morphology (e-f), microstructure within DLC:H-SiO counterpart (g-h).

adsorption of oxygen or moisture from the air. However, during run-in period, these oxides were worn away and extruded out of wear track. As shown in Fig. 5c, oxygen-containing material mainly originates from the counterpart surface in N_2. The content of sp^2-C in wear track of pre-graphitized coating significantly increased to 56.3%, while sp^3-C decreased to 29.9%, raising the sp^2-C/sp^3-C ratio to 1.9. This increasing trend is consistent with Raman data, indicating the transformation of sp^3-C to sp^2-C, which enhances graphitization at friction interface that promotes superlubrication. Owing to frictional heat and shear stress, the C-Si bond content further decreased to 3.2%.

The Si 2p spectrum exhibits four characteristic peaks shown in Fig. 5 (d, e, f). The peak at a binding energy of 100.5 eV is assigned to Si-C, while the peak at 101.4 eV is silicon oxycarbide (Si-O_2-C_2), an amorphous metastable phase in which silicon atoms are bonded to both oxygen and carbon atoms [42,43]. The peak at 102.5 eV is attributed to Si-O bonds. After pre-graphitization and friction tests, the content of Si-C bonds gradually decreased from 27.4% to 22.8%, accompanied by a reduction in Si-O_2-C_2 bonds. On one hand, thermal effects during high-vacuum annealing lead to the breaking of Si-C and Si-O_2-C_2 bonds of coating, promoting the formation of SiO_x clusters. On the other hand, mechanical stress and frictional heat during friction further facilitate the in situ formation of SiO_x phase [43]. The species observed at 103.5 eV, identified as Si-O_2·nH_2O, may result from adsorption of oxygen or moisture from the air after friction test. To examine the influence of N_2 on the friction interface and superlubricity performance during the friction, the evolution of chemical composition of N1s spectra under different states was conducted. Fig. 5(g) shows the as-deposited coating surface mainly contains minor amounts of N-N and N-H bonds that due to air adsorption. Fig. 5(h, i) reveal that trace N-N bonds remain after the heat treatment of the pre-graphitized coating, while trace amounts of N-Si bonds are generated after friction tests in an N_2 environment. This is attributed to the inert gas N_2, which makes it difficult to chemically combine with elements of coating surface. Therefore, N_2 primarily plays a protective role at the friction interface by inhibiting the ingress of gaseous oxygen and preventing the formation of oxidation products at interface.

3.5. The microstructure within pre-graphitized wear track

The worn internal structure of pre-graphitized coating along the sliding direction was characterized by high-resolution TEM to analyze the superlubricity behavior. As shown in Fig. 6a-b, the structure consists of Si-DLC:H layer and an intact gradient transition layer. The coating was worn downward along the thickness direction, with localized material loss at contact surface forming pit-like features. Due to repeated shear stress under loading, cracks initially nucleate at contact interface. Continued sliding promotes crack propagation along sliding direction. Upon reaching a critical size, adhered material was sheared off as wear debris, resulting in localized wear, this constitutes the fatigue wear mechanism of the coating. The diffraction rings shown in Fig. 6c-d are typical amorphous carbon halo and features of multiple large-sized nanocrystals, corresponding to Si-DLC:H and Cr/CrAlSiN layers, respectively.

Notably, the high-resolution image in Fig. 6e reveals a friction-induced loose layer enriched with sp^2-C in area 1, caused by the compression of powder-like debris in the wear track (Fig. 4). As illustrated in Fig. 6f, area 2 undergoes repeated shearing, peeling, adhesion, and compaction during sliding, accompanied by material transfer from the DLC:H-SiO counterpart and a few nanoparticles dispersed in the sp^2-C-rich layer on the worn surface. The overlapping O and Si elements in area 2 shown in Fig. 6b indicating the presence of irregular SiO_x nanoparticles—a finding consistent with XPS. The loosely friction layer in area 1 exhibits low shear strength and tends to undergo interlayer separation under shear stress. Fig. 6g-h reveals nanoparticles within and a loose layered structure in the locally magnified image of DLC:H-SiO counterpart, which likely serves as the primary source observed on the wear track surface. The structure composed of loose sp^2-C layered and SiO_x nanoparticles establishes a weak chemical bonding friction interface, thereby facilitating the achievement of superlubricity for Si-DLC:H coating in N_2.

3.6. Dynamic evolution of friction interfaces and lubricity mechanism

RMD was employed to investigate the dynamic evolution of the superlubricity interface and the lubricity mechanisms. The simulated friction interface of coating is shown in Fig. 7a, the upper layer is the counterpart surface, and the lower layer is coating surface. The Si atoms are uniformly distributed among C atoms of the as-deposited DLC:H coating, and chemical bonds of C-C, C-Si, and Si-Si are formed at interface. The friction forces (Fig. 7b) at interface show slightly differences, and the pre-graphited coating has lower friction force. For the as-deposited coating (Fig. 7c), the shear force will overcome the strong chemical bonds, resulting in high initial friction force during the initial 0–100 ps. As relative sliding continued from 200 to 1250 ps, clustering

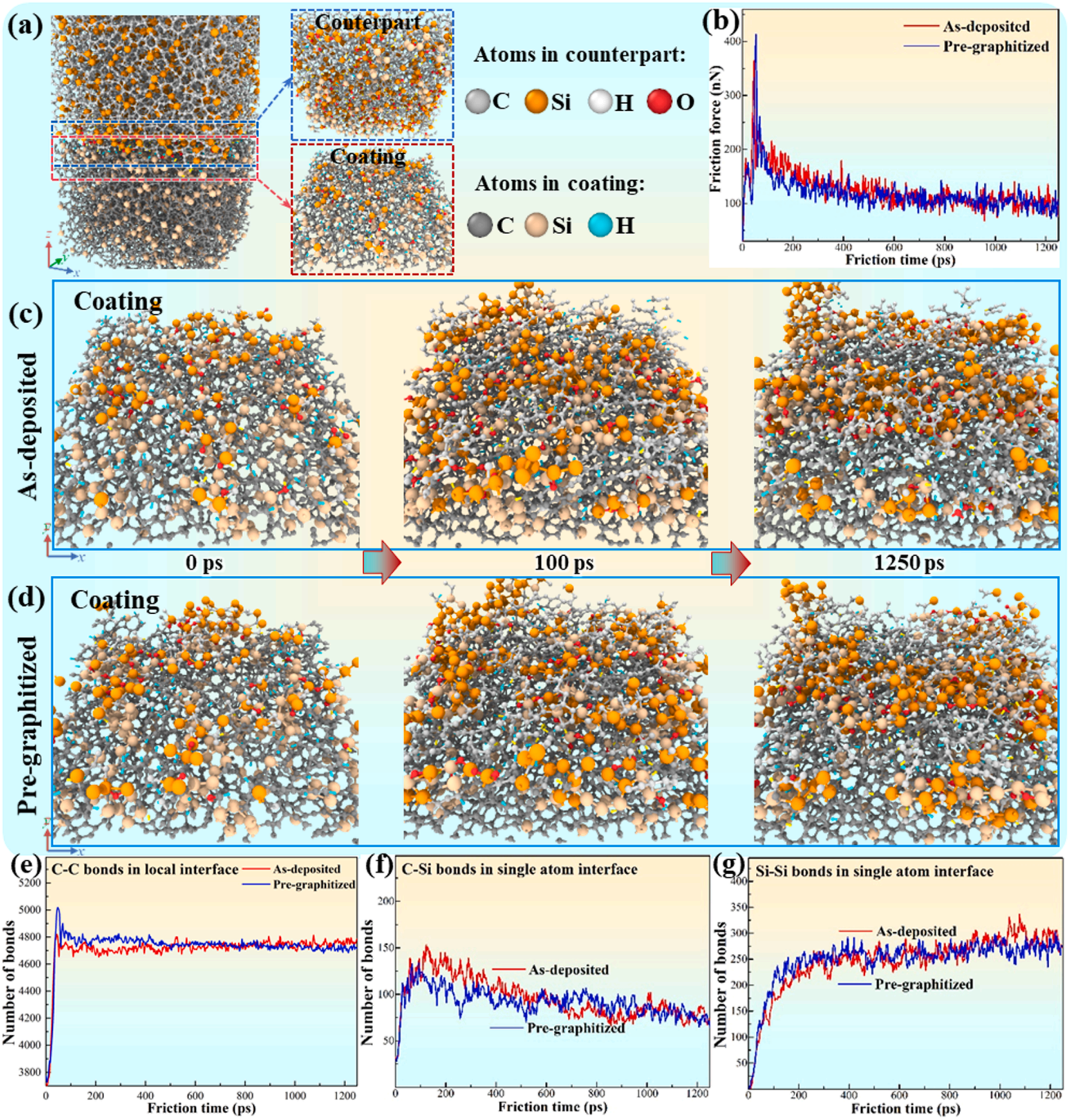


Fig. 7. Friction i*nterface model (a), friction force* (b), i*nterfacial morphologies of as-deposited (c) and pre-graphited (d) Si-DLC:H coatings;* contents of C-C bonds in local interface (e); contents of C-Si bonds (f), Si-Si bonds (g) at interface.

of Si/O atoms occurred and partial chemical bonds fractured at friction interface, and shear induced the reorganization of numerous chain-like SiO_x structures. The total C-C (65.4 kcal/mol) covalent bonds in local interface remained almost constant throughout, but the content of Si-C (31.6 kcal/mol) showed a trend of first increasing and then decreasing, while more Si-Si (23.2 kcal/mol) [44,45] bonds formed (Fig. 7e-g). Concurrently, the transformation of sp^3-C to sp^2-C in the interface resulted in the rapid decrease of friction force (Fig. S5d-e) and COF [22].

Fig. 7d presents friction interface of the pre-graphitized coating. A notable difference is the formation of SiOx clusters at the initial stage (0 ps). As shown in Fig. S5d-e, the initial sp^2 content after pre-graphitization was higher than that of the as-deposited coating, while the sp^3-C content exhibited the opposite trend. During the early sliding period (0–100 ps), C-Si bonds break and transform into more Si-Si bonds (Fig. 7f-g), resulting in a lower friction force than that of as-deposited coating [44,45].

Subsequently, shear-induced reorganization of the friction interface leads to the chain-like cluster structures from 100 ps to 1250 ps. This inhibits the formation of C-C bonds and promotes the transformation of hybrid carbon. Consequently, the sp^2-C content remains high, while the sp^3-C content continuously declines (Figs. S5d-e). The passivation of

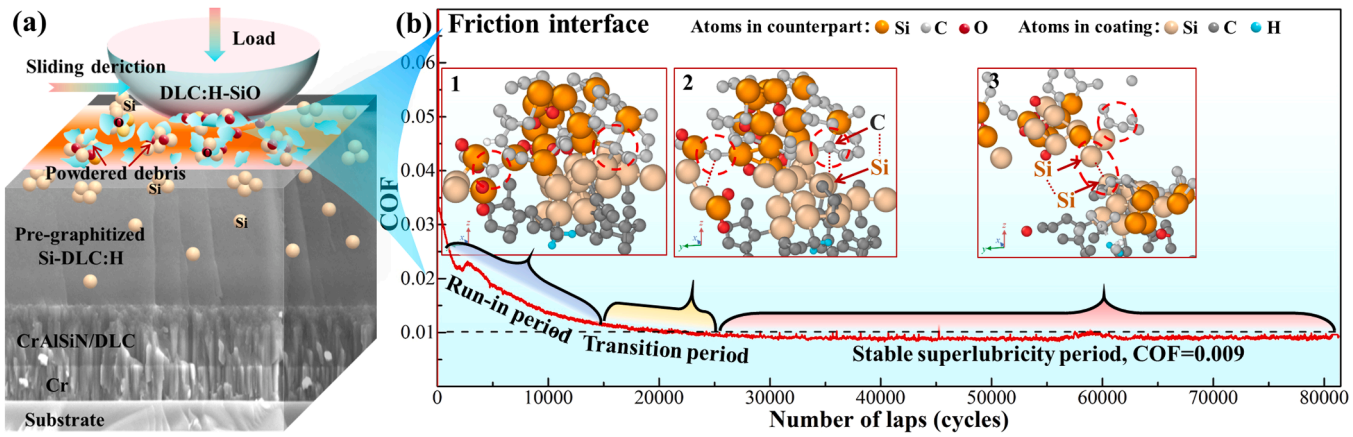


Fig. 8. The friction mechanism (a) and chemical bonds evolution (b) of pre-graphitized coating.

dangling bonds at the interface leads to a gradually decreasing and stabilizing friction curve and COF. After 500 ps of sliding, the morphology of the chain-like structures becomes similar for both coatings, leading to nearly identical friction forces, as also reflected by the synchronous convergence of the friction force curves and the quantities of interfacial C-C, C-Si and Si-Si bonds (Fig. 7b and Fig. S5). However, the pre-graphitized coating maintains a higher sp^2-C content throughout the entire friction stage, which enables it to achieve superlubricity (Fig. S5d). This consistent evolutionary trend suggests that the conversion of high-energy C-C and C-Si bonds into readily shearable Si-Si bonds is the key factor underlying the improved tribological performance.

The friction mechanism of pre-graphitized coating is illustrated in Fig. 8a, a formation of weakly chemically bonded friction interface that cluster nanoparticles dispersed in sp^2-C-rich powdery wear debris. From the perspective of atomic bonding in Fig. 8b1, shear forces remove the surface oxide layer during the run-in period and cause gradually wear of DLC:H-SiO counterpart, resulting in the formation of C-C, C-Si, Si-Si bonds at interface. As sliding continues, the friction interface undergoes graphitization and reorganization that the clusters are sheared off and evolve into chain-like structures. During the transition period as shown in Fig. 8b2, an interface formed dominated by increasing Si-Si and reducing Si-C contents, also suppresses more formation of strong C-C covalent bonds and construct a weak chemical bonding friction interface to reduce chemical interactions. Under shear force, more Si-C bonds fracture preferentially, the friction interface then evolves into a structure dominated by Si clusters interconnected by Si-Si bonds. Subsequently, the Si-Si bonds undergo shear-induced fracture as shown in Fig. 8b3. Simultaneously, the graphitization process causes the interface repulsion, characterized by the continuous transformation of sp^3-C to sp^2-C, coordinated weak chemical bonds break preferentially and eventually achieve stable superlubricity. Throughout the entire superlubricity period, the bonding and breaking of weak chemical bonds continuously occur until the end of friction. However, the quantitative contribution of each single factor cannot be separated due to simulation limitations.

4. Conclusions

This study successfully fabricated Si-DLC:H coating with strongly adherent, high hardness using HiPIMS-assisted ion beam technology. A friction interface reconstruction strategy was proposed, which combines surface pre-graphitization to establish a weak chemically bonded interface. During sliding, the worn counterpart generated highly graphitized, low-shear-strength powdery debris, consisting of SiO_x nanoparticles dispersed in a sp^2-C-enriched loose layer on the wear track. This interfacial structure enabled superlubricity and low W_R in N_2. RMD simulations further revealed that pre-graphitization promotes Si nanoparticles clustering and suppresses the formation of strong C-C covalent bonds at the interface. Instead, weak Si-Si bonds preferentially break, leading to a low-shear interface and reduced friction. Moreover, this work clarifies the crack initiation process and fatigue wear failure mechanism, elucidating both the atomic-scale dynamic evolution of the friction interface and the macroscopic superlubricity mechanism of Si-DLC:H coatings. These findings provide technical support for designing solid lubricant coatings and a theoretical basis for achieving superlubricity in critical moving components.

CRediT authorship contribution statement

Yupeng Zhang: Writing – review & editing, Writing – original draft, Methodology, Investigation, Funding acquisition, Formal analysis, Data curation. **Silong Zhang:** Validation, Software, Formal analysis. **Yanjin Li:** Validation, Formal analysis. **Rende Chen:** Validation, Methodology, Investigation, Formal analysis. **Gang Wen:** Investigation, Formal analysis. **Ming Qin:** Investigation, Formal analysis. **Peng Guo:** Validation, Investigation, Funding acquisition, Formal analysis. **Dae-Eun Kim:** Supervision, Investigation, Formal analysis. **Hao Li:** Validation, Formal analysis. **Aiying Wang:** Writing – review & editing, Supervision, Project administration, Funding acquisition, Conceptualization.

Declaration of Competing Interest

The authors declare that they have no known competing financial interests or personal relationships that could have appeared to influence the work reported in this paper.

Acknowledgements

This work was financially supported by the National Science Foundation of China (52505234, U24A2030). Leading Innovative and Entrepreneur Team Introduction Program of Zhejiang (2024R01004), Science and Technology Project of Zhejiang Province (2026C02A1253 (SD2)), and Major Special Project of Ningbo (2024Z134).

Statement of originality

We declare and guarantee this article is original and does not involve plagiarism with copyright infringement. The manuscript has not been published or submitted to another journal, neither in whole nor in parts.

Appendix A. Supporting information

Supplementary data associated with this article can be found in the

online version at doi:10.1016/j.triboint.2026.112870.

Data availability

Data will be made available on request.

References

[1] Li P, Ju P, Ji L, Li H, Liu X, Chen L, Zhou H, Chen J. Toward robust macroscale superlubricity on engineering steel substrate. Adv Mater 2020;32:2002039.
[2] Zhang Y, Li P, Ji L, Liu X, Wan H, Chen L, Li H, Jin Z. Tribological properties of MoS2 coating for ultra-long wear-life and low coefficient of friction combined with additive g-C3N4 in air. Friction 2021;9(4):789–801.
[3] Jang S, Chen Z, Kim SH. Origin of superlubricity of diamond-like carbon (DLC). Friction 2025;13(1):9440995.
[4] Hirano M, Shinjo K. Superlubricity and frictional anisotropy. Wear 1993;168(1):121–5.
[5] Wang Y, Deng W, Qi W, Chen X, Xu J, Zhang C. Understanding the interfacial behaviors during superlubricity process of a-C:H film coated on the rough bearing steel surface. Tribology Int 2022;171:107558.
[6] Wei X, Du N, Guo P, Chen R, Wu J, Wang L, Lee K-R, Li X, He H. Friction dependence on processing priority for graphitization/passivation coupled amorphous carbon films. Carbon 2024;230:119631.
[7] Ma L, Nemati N, Kim DE, Aghababaei R. Interface Amorphization Controls Maximum Wear Resistance of Multinanolayer DLC/WC Coatings. ACS Appl Mater Interfaces 2024;16(14):18090–8.
[8] Yu Q, Chen X, Zhang C, Zhang C, Deng W, Wang Y, Xu J, Qi W. Ion energy-induced nanoclustering structure in a-C:H film for achieving robust superlubricity in vacuum. Friction 2022;10(12):1967–84.
[9] Zhu D, Zhang J, Li P, Li Z, Li H, Liu X, Ma T, Ji L, Zhou H, Chen J. Robust macroscale superlubricity in humid air via designing amorphous DLC/crystalline TMDs friction pair. Adv Funct Mater 2024;34:2316036.
[10] Erdemir A, Eryilmaz O, Fenske G. Synthesis of diamondlike carbon films with superlow friction and wear properties. Journal Vacuum Science & Technology A Vacuum Surfaces Films 2000;18(4):1987–92.
[11] Yang Y, Chen Y, Han T, Shang L, Liu B, Pan M, Liang Y, Chen X. Evolution of interfacial nanostructures with temperature governing fretting wear in diamond-like carbon films. Carbon 2024;226:119217.
[12] Chen Z, Wei X, Lu S, Ding J, Du N, Feng C, Chen K, Guo P, Lee K-R, Zhang G, Li X. Surface in-situ graphitization and properties of amorphous carbon film induced by laser irradiation. Friction 2025;13:9440977.
[13] Yu Q, Chen X, Zhang C, Tian J, Deng W, Huang P. Extreme contact pressure-induced in-situ structural evolution of nanoclusters governing macroscopic superlubricity in a-C:H films. Carbon 2023;215:118457.
[14] Wang J, Pu J, Zhang G, Wang L. Architecture of superthick diamond-like carbon films with excellent high temperature wear resistance. Tribology Int 2015;81:129–38.
[15] Liu Y, Zhang H. The synergistic mechanism between graphitized tribofilm and graphitized surface of diamond-like carbon film under different temperature environments. Diam Relat Mater 2022;123:108875.
[16] Chen X, Kato T. Growth mechanism and composition of ultrasmooth a-C:H:Si films grown from energetic ions for superlubricity. J Appl Phys 2014;115(4).
[17] Wang K, Yang B, Zhang B, Bai C, Mou Z, Gao K, Yushkov G, Oks E. Modification of a-C:H films via nitrogen and silicon doping: The way to the superlubricity in moisture atmosphere. Diam Relat Mater 2020;107:107873.
[18] Zhang TF, Wan ZX, Ding JC, Zhang S, Wang QM, Kim KH. Microstructure and high-temperature tribological properties of Si-doped hydrogenated diamond-like carbon films. Appl Surf Sci 2018;435:963–73.
[19] Jiang X, Guo P, Cui L, Zhang Y, Chen R, Ye Y, Wang A, Ke P. Tribological behavior of silicon and oxygen co-doped hydrogenated amorphous carbon coatings on polyether ether ketone. Diam Relat Mater 2023;132:109650.
[20] Yin Z, Yu Y, Chen H, Li J, Bai L. Nanofriction behaviors between silicon-doped diamond-like carbon films under different testing conditions. Comput Mater Sci 2021;188:110182.
[21] Deng W, Wang Y, Yu Q, Chen X, Huang P, Yu X, Qi W, Li X, Zhang C, Luo J. Genesis of Superlow Friction in Strengthening Si-DLC/PLC Nanostructured Multilayer Films for Robust Superlubricity at Ultrahigh Contact Stress. ACS Appl Mater Interfaces 2022;14(45):51564–78.
[22] Li X, Du N, Feng C, Chen K, Wei X, Zhang D, Lee K-R. Theoretical superlubricity and its friction stability of amorphous carbon film induced by simple surface graphitization. Appl Surf Sci 2023;615:156318.
[23] Pei L, Chen W, Ju P, Zhou H, Xu Z, Ji L, Ma T, Li H, Liu X, Zhou H, Chen J. Regulating vacuum tribological behavior of a-C:H film by interfacial activity. J Phys Chem Lett 2021;12(42):10333–8.
[24] Plimpton S. Fast Parallel Algorithms for Short-Range Molecular Dynamics. J Comput Phys 1995;117(1):1–19.
[25] Van Duin AC, Dasgupta S, Lorant F, Goddard WA. ReaxFF: a reactive force field for hydrocarbons. J Phys Chem A 2001;105(41):9396–409.
[26] Berendsen HJC, Postma JPM, Van Gunsteren WF, Dinola A, Haak JR. Molecular dynamics with coupling to an external bath. J Chem Phys 1984;81(8):3684–90.
[27] Li X, Wang A, Lee K-R. Mechanism of contact pressure-induced friction at the amorphous carbon/alpha olefin interface. npj Comput Mater 2018;4(1):53.
[28] Li X, Wang A, Lee K-R. Insights on low-friction mechanism of amorphous carbon films from reactive molecular dynamics study. Tribology Int 2019;131:567–78.
[29] Ma T-B, Hu Y-Z, Wang H. Molecular dynamics simulation of shear-induced graphitization of amorphous carbon films. Carbon 2009;47(8):1953–7.
[30] Kuwahara T, Romero PA, Makowski S, Weihnacht V, Moras G, Moseler M. Mechano-chemical decomposition of organic friction modifiers with multiple reactive centres induces superlubricity of ta-C. Nat Commun 2019;10(1):151.
[31] Zhang S, Li X, Guo P, Zhang X, Li H, Chen R, Wang Z, Nishimura K, Wang A. Pressure-regulated tribology of a-C/PEEK friction pair under deep-sea environment: Interfacial evolution and atomic-scale simulation. Tribology Int 2026;223:112233.
[32] Wang Y, Xu J, Zhang J, Chen Q, Ootani Y, Higuchi Y, Ozawa N, Martin JM, Adachi K, Kubo M. Tribochemical reactions and graphitization of diamond-like carbon against alumina give volcano-type temperature dependence of friction coefficients: A tight-binding quantum chemical molecular dynamics simulation. Carbon 2018;133:350–7.
[33] Wang Y, Xu J, Ootani Y, Bai S, Higuchi Y, Ozawa N, Adachi K, Martin JM, Kubo M. Tight-Binding Quantum Chemical Molecular Dynamics Study on the Friction and Wear Processes of Diamond-Like Carbon Coatings: Effect of Tensile Stress. ACS Appl Mater & Interfaces 2017;9(39):34396–404.
[34] Hahn SH, Rimsza J, Criscenti L, Sun W, Deng L, Du J, Liang T, Sinnott SB, Van Duin ACT. Development of a ReaxFF Reactive Force Field for NaSiOx/Water Systems and Its Application to Sodium and Proton Self-Diffusion. J Phys Chem C 2018;122(34):19613–24.
[35] Zhang Y, Wang Z, Guo P, Wang A, Ke P. Enhanced tribological behavior of VAlN hard ceramic coating with intermittent amorphous carbon layer. Ceram Int 2023;49(10):15091–100.
[36] Zhang Y, Wang Z, Zhou S, Zhang Y, Dong Y, Wang A, Ke P. Synergistic effect of V and Ag diffusion favored the temperature-adaptive tribological behavior of VAlN/Ag multi-layer coating. Tribology Int 2024;192:109285.
[37] Li J, Kim SJ, Han S, Chae H. Characterization of sp2/sp3 hybridization ratios of hydrogenated amorphous carbon films deposited in C2H2 inductively coupled plasmas. Surf Coat Technol 2021;422:127514.
[38] Ferrari AC, Robertson J. Interpretation of Raman spectra of disordered and amorphous carbon. Phys Rev B 2000;61(20):14095.
[39] Dwivedi N, Yeo RJ, Zhang Z, Dhand C, Tripathy S, Bhatia CS. Interface Engineering and Controlling the Friction and Wear of Ultrathin Carbon Films: High sp3 Versus High sp2 Carbons. Adv Funct Mater 2016;26(10):1526–42.
[40] Jin B, Du N, Meng T, Chen G, Cao Y, Zhang H, He Y, Li X, Zhang C, Yu X, Zeng Q, Luo J. High contact stress phase transition structural superlubricity. Carbon 2025;238:120306.
[41] Deng W, Wang Y, Chen X, Qi W, Li X, Zhang C, Yu Q, Xu J. Design architecture of colorful Si-DLC/PLC nanostructured multilayer films for robust superlubricity at high contact stress in dry N2 atmosphere. Appl Surf Sci 2022;595:153535.
[42] Shimoda K, Park J-S, Hinoki T, Kohyama A. Influence of surface structure of SiC nano-sized powder analyzed by X-ray photoelectron spectroscopy on basic powder characteristics. Appl Surf Sci 2007;253(24):9450–6.
[43] Chen J, Song W, Li J. Macroscopic superlubricity achieved by hydrolysis reaction of ethyl lactate on silicon-doped diamond-like carbon film. Carbon 2024;230:119675.
[44] Yl W, Ra P. Generalized valence bond study of rotational singlet structures and pi bond energies for systems containing C = C, Si = Si, and C = Si double bonds. Can J Chem 1998;(4):477–82.
[45] Jian W, Kaiming Z, Xide X. Pair potentials for C-C, Si-Si and Si-C from inversion of the cohesive energy. J Phys Condens Matter 1994;6(5):989–96.